Materials Research Bulletin 49 (2014) 572–576

Contents lists available at ScienceDirect

Materials Research Bulletin

journal homepage: www.elsevier.com/locate/matresbu

Rapid preparation of α-FeOOH and α-Fe_2O_3 nanostructures by microwave heating and their application in electrochemical sensors

J.Z. Marinho [a], R.H.O. Montes [a], A.P. de Moura [b], E. Longo [b], J.A. Varela [b], R.A.A. Munoz [a], R.C. Lima [a,*]

[a] Universidade Federal de Uberlândia, Instituto de Química, 38400-902 Uberlândia, MG, Brazil
[b] Universidade Estadual Paulista, Instituto de Química, 14800-900 Araraquara, SP, Brazil

ARTICLE INFO

Article history:
Received 24 January 2013
Received in revised form 7 September 2013
Accepted 29 September 2013
Available online 8 October 2013

Keywords:
A. Oxides
B. Chemical synthesis
C. X-ray diffraction
C. Electron microscopy
D. Electrochemical properties

ABSTRACT

α-FeOOH (goethite) and α-Fe_2O_3 (hematite) nanostructures have been successfully synthesized using the microwave-assisted hydrothermal (MAH) method and by the rapid burning in a microwave oven of the as-prepared goethite, respectively. The orthorhombic α-FeOOH to rhombohedralα-Fe_2O_3 structural transformation was observed by X-ray diffraction (XRD) and Raman spectroscopy results. Plates-like α-FeOOH prepared in 2 min and rounded and quasi-octahedral shaped α-Fe_2O_3 particles obtained in 10 min were observed using field emission gun scanning electron microscopy (FE-SEM) and transmission electron microscopy (TEM). The use of microwave heating allowed iron oxides to be prepared with shorter reaction times when compared to other synthesis methods. α-FeOOH nanoplates were incorporated into graphite-composite electrodes, which presented electrocatalytic properties towards the electrochemical oxidation of ascorbic acid in comparison with unmodified electrodes. This result demonstrates that such α-FeOOH nanostructures are very promising chemical modifiers for the development of improved electrochemical sensors.

1. Introduction

Over the past decade, there has been increasing interest in the synthesis of metal oxides semiconductor nanomaterials with well-controlled shapes and sizes, due to their unique chemical and physical properties; which are helpful in a wide range of application such as photonics, photoelectronics, sensors and catalysis [1,2]. Iron (III) oxide has four principal polymorphs, hematite (α-Fe_2O_3), maghemite (γ-Fe_2O_3), β-Fe_2O_3 and ε-Fe_2O_3; iron (III) oxy-hydroxide also has four known as goethite (α-FeOOH), akaganéite (β-FeOOH), lepidocrocite (γ-FeOOH) and feroxyhyte (δ-FeOOH) [3]. In particular, α-$Fe_2O_3$is a significant n-type semiconductor, E_g = 2.1 eV, with excellent chemical stability and low toxicity under ambient conditions [4]. Among these oxides, α-FeOOH and α-Fe_2O_3 have been widely investigated in magnetic devices, catalysts, pigment production, gas sensors and photoelectrodes [5–7].

Among the several methods of iron oxide synthesis, such as microemulsion [8], chemical vapour deposition [9], co-precipitation [10,11], solvothermal [12], hydrothermal [13–17], ultrasonic hydrothermal [18], and microwave irradiation [19,20], the microwave-assisted hydrothermal (MAH) method [21–23] occupies a prominent position, due to its advantages over other synthesis processes. The hydrothermal technique has been employed in the preparation of α-FeOOH and α-Fe_2O_3 powders as an efficient low-temperature method, however the synthesis is very slow at any temperature. Hydrothermal conditions combined with microwave heating can increase the kinetics of crystal growth [24] and result in the extremely rapid synthesis of micro- or nano-scale dimensioned materials by a rate one and two increases in magnitude [25–27]. In particular, the MAH method offers synthesis with a short reaction time at low temperature, low power consumption and with no air pollution [28–30]. The main advantage over other methods of synthesis is the uniform and fast heating of the reaction environment.

Herein, we report on the rapid preparation of the iron oxy-hydroxide (α-FeOOH) nanostructures in aqueous solution using the (MAH) method for 2 min without the addition of surfactants or other additives, and of α-Fe_2O_3 nanoparticles by burning for 10 min of the as-prepared precursor in a domestic microwave oven. The phase transformation was verified by X-ray diffraction (XRD) patterns, and the samples were characterized by field emission gun scanning electron microscopy (FE-SEM), transmission electron microscopy (TEM), Raman spectroscopy and UV–vis absorbance. The α-FeOOH nanostructures obtained were incorporated

* Corresponding author at: João Naves de Ávila, 2121, Bairro Santa Mônica, CEP 38400-902 Uberlândia, MG, Brazil. Tel.: +55 34 3239 4143; fax: +55 34 3239 4143.
E-mail address: rclima@iqufu.ufu.br (R.C. Lima).

0025-5408/$ – see front matter © 2013 Elsevier Ltd. All rights reserved.
http://dx.doi.org/10.1016/j.materresbull.2013.09.052

into a graphite-composite electrode and their electrocatalytic activity was evaluated with respect to the electrochemical oxidation of ascorbic acid.

2. Materials and methods

2.1. Synthesis of α-FeOOH and α-Fe_2O_3nanostructures

All chemicals reagents are of analytical grade and were used without further treatment: 2×10^{-3} mol of $Fe(NO_3)_3{\cdot}9H_2O$ was dissolved in 40 mL of distilled water under vigorous stirring. Then, 2.0 mol/L KOH solution was added to adjust the pH to 12 under constant stirring for 15 min. The suspension was transferred into a 50 mL Teflon autoclave and heated in a microwave oven at 140 °C for 2 min. The yellowish-brown solid obtained was washed several times with distilled water and ethanol and dried at 60 °C. Finally, reddish-brown powders were obtained by the heating of the as-prepared precursor in a domestic microwave oven at 350 °C for 10 min.

2.2. Characterization of samples

The powders obtained were structurally characterized by XRD using a Shimadzu XRD 6000 (Japan) equipped with CuKα radiation (λ = 1.5406 Å), in the 2θ range from 10° to 80° with a 0.02°/min scan increment. The morphology was investigated by FE-SEM (Supra 35-VP, Carl Zeiss, Germany). Transmission electron microscopy (TEM) images and selected-area electron diffraction (SAED) patterns were taken on a FEI Tecnai G2F20 transmission electron microscope with accelerating voltage of 200 kV. Raman spectra were recorded on a RFS/100/S Bruker Fourier Transform Raman (FT-Raman) spectrometer. The 1064 nm line of a Nd:YAG ion laser was used as the excitation source; the power was kept at 55 mW. UV–vis spectra were recorded at room temperature on a Cary 5G spectrophotometer fitted with an integrating sphere. The spectra were referenced against the compressed $BaSO_4$ powder.

2.3. Preparation of α-FeOOH-modified graphite-composite electrodes and electrochemical measurements

α-FeOOH nanostructures were added to the pure graphite (Ø: 1–2 μm, Sigma–Aldrich, Milwaukee, USA) in the mass proportion of 10/90 (α-FeOOH/pure graphite), and then mixed with Araldite® epoxy adhesive (Brascola, Joinville, Brazil) and cyclohexanone (Vetec, Rio de Janeiro, Brazil) and stirred for 24 h in order to obtain a homogeneous graphite-composite fluid. The fluid was inserted into a polyamide tube ($\varnothing_i$ = 7.2 mm) in which a copper wire was previously set (electrical contact). The cure time was 24 h at room temperature. After that, the electrode was polished with 400 and 1200 grit sand paper in the presence of water. Before the cyclic voltammetry measurements of ascorbic acid (Sigma–Aldrich), the composite electrode was submitted to a cyclic voltammetry experiment in the range of −0.4 and +0.8 V in a 0.05 mol L^{-1} phosphate buffer solution (pH = 7.2, K_2HPO_4/KH_2PO_4, supporting electrolyte) at 50 mV s^{-1} for 40 cycles. The electrochemical measurements were performed using a μ-Autolab Type III (Eco Chemie, Utrecht, Netherlands) controlled by GPES4.9.007 software (General Purpose Electrochemical System). Cyclic voltammograms measurements were performed in a conventional three-electrode electrochemical cell (12 mL) at room temperature. The working, counter, and reference electrodes were, respectively, iron(III) oxy-hydroxide (α-FeOOH)-modified (or unmodified) graphite-composite electrode, platinum wire, and Ag/AgCl/saturated KCl.

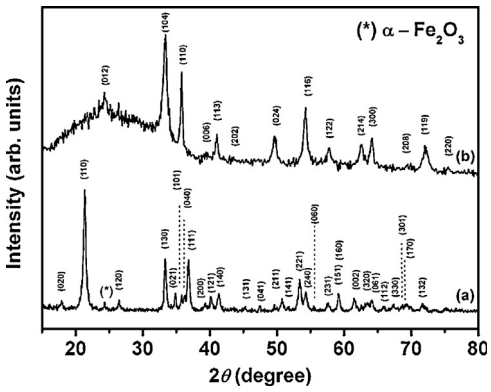

Fig. 1. Powder X-ray diffraction patterns of (a) α-FeOOH synthesized by MAH method and (b) α-Fe_2O_3 obtained from as-prepared precursor heating in microwave oven.

3. Results and discussion

Fig. 1 shows the X-ray diffraction patterns of the powders obtained using the MAH method followed by heating in a microwave oven. All the diffraction peaks in Fig. 1(a) can be indexed to orthorhombic α-FeOOH structure with lattice constants, a = 4.61 Å, b = 9.95 Å and c = 3.02 Å and space group $P2_1nm$, which are consistent with the standard card goethite, JCPDS no. 29-0713. The sharp diffraction peaks indicate the formation of a crystalline α-FeOOH structure obtained over 2 min using the MAH method. When the as-prepared goethite sample was heated under microwave radiation the rhombohedral α-Fe_2O_3 structure was formed. The XRD patterns of typical α-Fe_2O_3 are shown in Fig. 1(b), in which the peaks positions are according to planes indexed to the hematite structure (JCPDS no. 33-0664). The high crystallinity of the α-Fe_2O_3 sample is observed by its narrow peaks (Fig. 1(b)). Some hematite traces are observed in this sample as indicated in

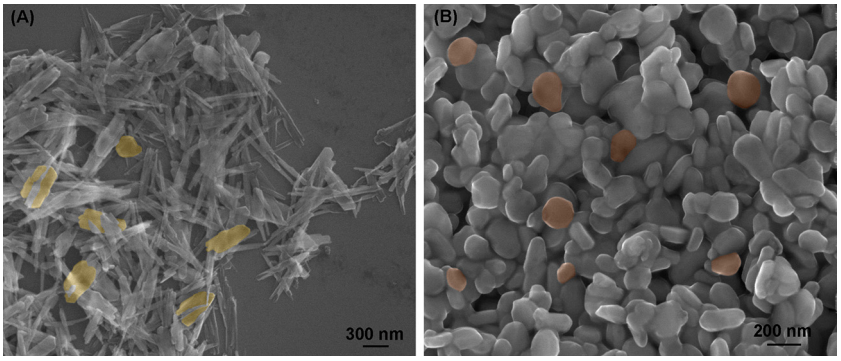

Fig. 2. FE-SEM images of (A) α-FeOOH obtained by MAH method for 2 min and (B) α-Fe_2O_3 obtained by as-prepared precursor heating in microwave oven.

Table 1
Iron (III) oxide species obtained under different synthesis conditions.

Synthesis method/reaction time	Product 1	Heating conditions	Product 2	Ref.
Glucose-guided hydrolyzing approach/12 h	α-FeOOH	Conventional oven/300 °C for 1 h	α-Fe_2O_3	[31]
Conventional hydrothermal/12 h	α-FeOOH + α-Fe_2O_3	Conventional oven/250 °C for 30 min	α-Fe_2O_3	[32]
Solution-based method/40 °C – until 1 h	α-FeOOH	Conventional oven/500 °C for 3 h	α-Fe_2O_3	[33]
Air oxidation/not described	α-FeOOH	Conventional oven/275 °C for 20 min to 4 h	α-Fe_2O_3	[34]
Microwave-hydrothermal/2 min	α-FeOOH	Domestic microwave oven/350 °C for 10 min	α-Fe_2O_3	This work

Fig. 1(a). The goethite–hematite phase transformation was observed, indicating that the α-FeOOH precursor was totally transformed into α-Fe_2O_3.

The morphology of the samples was studied by FE-SEM and TEM. Fig. 2(a) shows the FE-SEM image of α-FeOOH prepared by the MAH method at 140 °C. The sample is constituted of a great quantity of homogeneous products, forming irregular plate-like nanostructures of about 260 nm. This iron(III) oxy-hydroxide can also be prepared by a conventional hydrothermal method and other synthesis methods with a long reaction time, as presented in Table 1. Herein, α-FeOOH powders with uniform nanostructures and thin thicknesses of 50 nm were obtained in aqueous solution for 2 min without the addition of surfactants.

The FE-SEM image (Fig. 2(b)) shows the α-Fe_2O_3 powders prepared by as-prepared α-FeOOH burning in a microwave oven. The microwave heating quickly produces α-Fe_2O_3 particles with a rounded shape and with a hexagonal irregular shape, with a quasi-octahedral shape similar to the hexagonal crystal structure of the hematite formed. A coalescence of nano-particles can be observed from microwave annealing. The heating of the as-prepared α-FeOOH using a microwave is faster when compared to burning in a conventional oven, as shown in Table 1. α-Fe_2O_3 powders can also be obtained directly from the conventional hydrothermal method with a long reaction time [35–37]. With the use of a domestic microwave oven the α-Fe_2O_3 nano-size particles of about 160 nm were obtained quickly after 10 min of heating. This occurs because in the microwave burning process the sample is directly heated, accelerating the formation and crystallization of the material. The mechanism of energy transfer using a microwave process is different from the other heating mechanisms of the three established modes of heat transfer: conduction, convection and radiation [38,39]. In a liquid state, the microwave-hydrothermal combination results in the homogenous nucleation and rapid growth of particles [40–42]. Rapid heating under certain internal pressures produce a high mobility of dissolved ions, increasing the collision rate of particles, which leads to the rapid formation of the compound, as shown in the α-FeOOH preparation.

TEM and selected-area electron diffraction (SAED) results reveal the phase transformation of α-FeOOH into α-Fe_2O_3 nanoparticles. Fig. 3(A) displays the typical TEM image of the as-synthesized α-FeOOH nanostructures, which indicates that the obtained products consisted of thin plates. The SAED pattern in the inset image of Fig. 3(A) reveals the highly crystalline nature of α-FeOOH, which is also in agreement with the XRD results. A change of morphology of α-FeOOH to α-Fe_2O_3 sample is observed in TEM images, Fig. 3(B), as shown by FE-SEM images. The inset showing the select area electron diffraction (SAED) pattern of the α-Fe_2O_3 particles indicates high crystallinity of the sample, which can be indexed to the pure rhombohedral phase of hematite α-Fe_2O_3.

Raman microscopy is sensitive to structural changes and was used to identify the goethite to hematite phase transformation, as observed in Fig. 4. The band positions for the α-FeOOH sample are in range 242, 298, 389, 478 and 555 cm^{-1}, which are characteristic of goethite structure with two strong peaks at 298 and 389 cm^{-1} [43], as shown in Fig. 4(a). The formation of the rhombohedral α-Fe_2O_3 structurefrom the as-prepared α-FeOOH sample heated in a microwave oven is verified in Fig. 4(b). The typical Raman peaks of the hematite structure which belong to the D^6_{3d} crystal space group [44] are observed, and six phonon lines can be assigned to the spectrum: the peaks at 224 and 498 cm^{-1} belong to A_{1g} symmetry and the other five peaks belong to E_g symmetry species in the region 245, 294, 409, 610 cm^{-1} [45]. The magnitude of the distortions into α-Fe_2O_3 can be sufficient to appreciably widen the frequency ranges. The peaks in the Raman spectrum of the α-Fe_2O_3 powders became proportionally narrower, indicating a better crystallized sample. The Raman spectra are in agreement with the structural changes observed by XRD.

The UV–vis absorption spectra of the α-FeOOH and α-Fe_2O_3 powders are shown in Fig. 5. The UV–vis spectra of goethite and hematite are similar and the band energies are essentially the

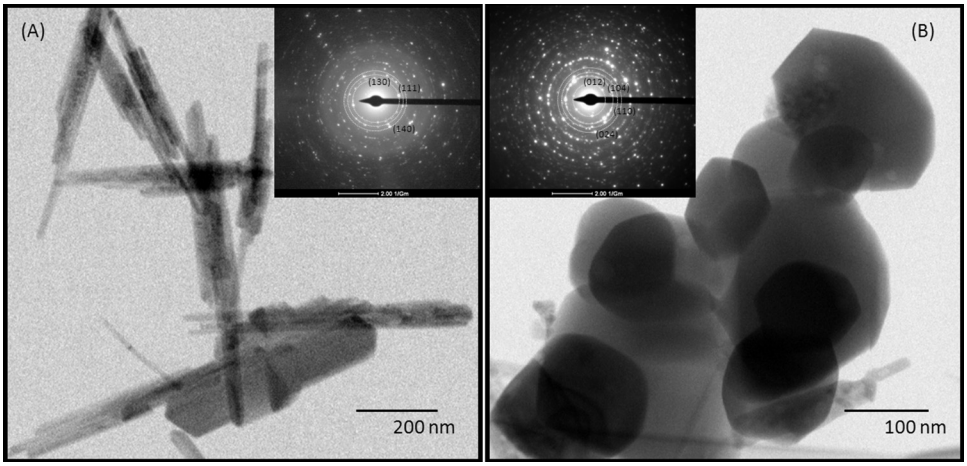

Fig. 3. TEM images of (A) α-FeOOH synthesized by MAH method (inset: SAED pattern) and (B) α-Fe_2O_3 obtained from as-prepared precursor heating in microwave oven (inset: SAED pattern).

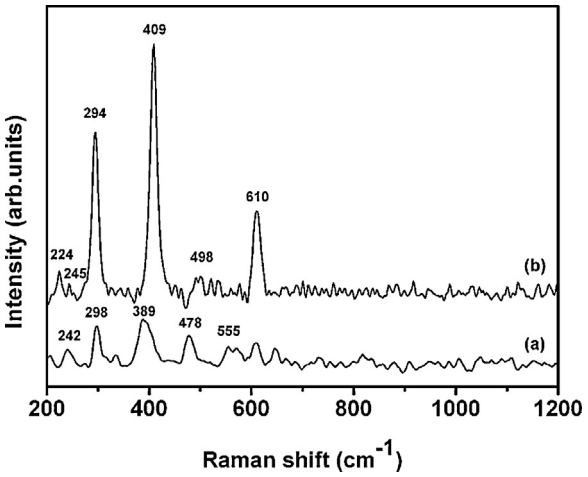

Fig. 4. Raman spectra of nanostructures (a) α-FeOOH and (b) α-Fe_2O_3obtained from as-preparedα-FeOOH.

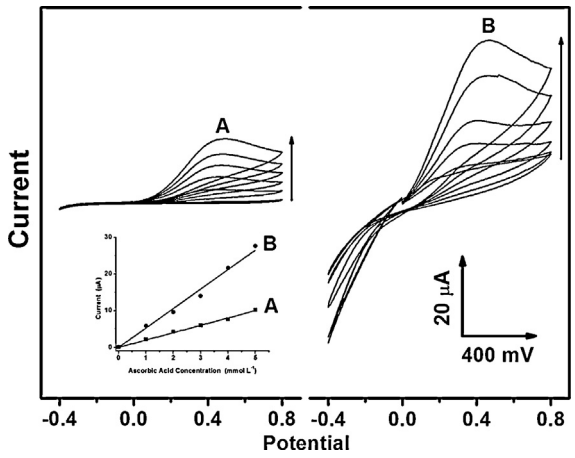

Fig. 6. Cyclic voltammetric measurements for increasing concentrations of ascorbic acid (1–5 mmol L^{-1}) at (A) unmodified and (B) modified graphite-composite electrodes with α-FeOOH nanoplates. Inset: the respective calibration curves. Arrows indicate the increase of current signal for increasing concentrations of ascorbic acid.

same, as observed in Fig. 5(a) and (b). The magnetic coupling of adjacent Fe^{3+} cations in the structures of these oxides is responsible for the strong intensity of the Fe^{3+} ligand field transitions [46]. The absorption bands at around 285 and 390 nm are assigned to $^6A_{1g} \rightarrow {}^4T_{1g}$ (^4P) and $^6A_{1g} \rightarrow {}^4E$ (^4D) from the ligand to metal charge-transfer transitions and contributions of the Fe^{3+} ligand field transitions. The strong absorption in the region near to 535 nm is attributed to overlapped contributions of $^6A_{1g} \rightarrow {}^4E_g$, $^4A_{1g}$ (^4G) ligand field transitions [47]. The colour variation of yellowish-brown goethite and reddish-brown hematite phase results from the higher energy Fe^{3+} ligand field transitions and Fe^{3+}–Fe^{3+} pair transitions via the magnetic coupling of neighbouring Fe^{3+}ions.

Fig. 6 presents the cyclic voltammetric measurements for the electrochemical oxidation of ascorbic acid at (A) unmodified and (B) modified graphite-composite electrodes with α-FeOOH nanoplates and their respective calibration curves (inset).

The cyclic voltammetry recordings (A) revealed an oxidation peak starting at 150 mV, attributed to the electrochemical oxidation of ascorbic acid at the unmodified graphite-composite electrode. The electrochemical oxidation of ascorbic acid at the modified electrode (B) is anticipated (150 mV), occurring at 0 mV. In addition, a substantial current increase (compared to the unmodified electrode) was verified. The calibration curves obtained for ascorbic acid using the cyclic voltammetry data clearly indicate the higher sensitivity (slopes for A and B were 1.980 and 5.421 μA L $mmol^{-1}$, respectively) of the modified electrode (around 3-fold).

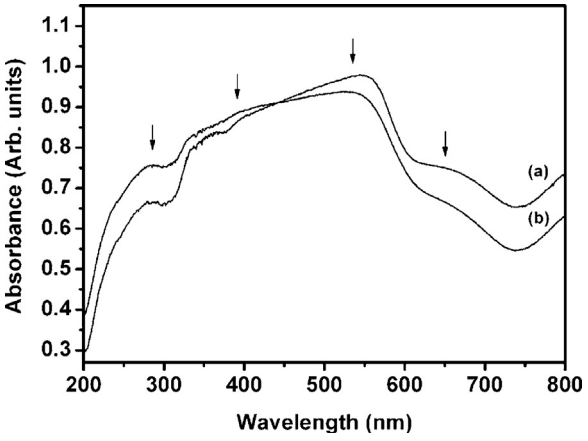

Fig. 5. UV–vis spectra of nanostructures (a) α-FeOOH and (b) α-Fe_2O_3.

The cyclic voltammetry recordings demonstrated that the modified graphite-composite electrode containing α-FeOOH nanostructures improved the electrochemical response to ascorbic acid. The lowered oxidative potential (150 mV) and significant current increase may be related to the electrocatalytic properties of α-FeOOH nanostructures. α-FeOOH acts as a mediator for the electrochemical oxidation of ascorbic acid [48]. Fe(III) at the surface of the modified electrode is reduced to Fe(II) by ascorbic acid, which is then oxidized forming dehydroascorbic acid. As long as the potential is swept to positive values, Fe(II) is re-oxidized to Fe(III), and then the electrode surface of the modified electrode is regenerated. The electrochemical oxidation of ascorbic acid at modified graphite-composite electrodes with α-Fe_2O_3 nanoparticles was also investigated (voltammograms not shown). It was also observed a similar decrease in the oxidation potential (150 mV) to ascorbic acid; however, there was no current increase in comparison with unmodified graphite-composite electrodes. Probably, the morphology and size of both nanostructures play key role on the enhancement of oxidation current verified at the modified graphite-composite electrodes with α-FeOOH nanoplates.

Modified electrodes with a copolymer of aniline with Fe(III)-porphyrin [49] and with single-walled carbon nanotubes containing Fe_2O_3 nanoparticles [50] did not present similar responses to ascorbic acid as presented by the modified-electrode proposed. Graphite-composite electrodes modified with such a nanostructured material are under investigation in the electrochemical oxidation and reduction of other analytes due to its promising electrocatalytic properties.

4. Conclusions

Microwave heating has demonstrated to be an appropriate and environmentally friendly process in the quick preparation of iron(III) oxide and oxy-hydroxide crystalline nanostructures. The complete transformation of the goethite to hematite phases in a short reaction time was observed and characterized by DRX and Raman techniques. Nano-plates and rounded nanoparticles were revealed by FE-SEM images. The UV–vis spectra of both oxides show bands corresponding to the Fe^{3+} ligand field and ligand-to-metal charge-transfer transitions and the very intense Fe^{3+} ligand field and Fe^{3+}–Fe^{3+} pair transitions responsible for the colour variation in the species. FE-SEM illustrated the plates-like

morphology α-Fe_2O_3 and α-FeOOH. The graphite-composite electrode modified with α-FeOOH nanostructures provided improved electrochemical responses (higher current and lower oxidative potential) towards ascorbic acid, which can be attributed to the electroatalytic properties of the α-FeOOH nanostructures. Such nanostructured chemical modifiers offer great promise in the development of improved electrochemical sensors.

Acknowledgements

The authors are grateful to CNPq (477150/2008-0), FAPEMIG (APQ-01842-09) and CAPES and Rede Mineira de Química (RQ-MG) by the financial support.

References

[1] C. Burda, X.B. Chen, R. Narayanan, M.A. El-Sayed, Chem. Rev. 105 (2005) 1025–1102.
[2] J.K. Dongre, M. Ramrakhiani, J. Alloys Compd. 487 (2009) 653–658.
[3] T. Hanslìk, J. Tláskal, J. Šubrt, V. Zapletal, Mater. Chem. 6 (1981) 267–276.
[4] L. Song, S. Zhang, Colloids Surf. A, 348 (2009) 217–220.
[5] B.C. Faust, M.R. Hoffmann, D.W. Bahnemann, J. Phys. Chem. 93 (1989) 6371–6381.
[6] S.K. Mohapatra, S.E. John, S. Banerjee, M. Misra, Chem. Mater. 21 (2009) 3048–3055.
[7] C. Wu, P. Yin, X. Zhu, C. OuYang, Y. Xie, J. Phys. Chem. B 110 (2006) 17806–17812.
[8] F. Geng, Z. Zhao, H. Cong, J. Geng, H.-M. Cheng, Mater. Res. Bull. 41 (2006) 2238–2243.
[9] Y. Zhou, Z.J. Zhang, Y. Yue, Mater. Lett. 59 (2005) 3375–3377.
[10] Z.-G. Wu, J.-F. Gao, Micro. Nano Lett. 7 (2012) 533–535.
[11] S. Rajendran, V.S. Rao, H.S. Maiti, J. Solid State Chem. 53 (1984) 227–235.
[12] M.-T. Liang, S.-H. Wang, Y.-L. Chang, H.-I. Hsiang, H.-J. Huang, M.-H. Tsai, W.-C. Juan, S.-F. Lu, Ceram. Int. 36 (2010) 1131–1135.
[13] H. Zhu, D. Yang, L. Zhu, H. Yang, D. Jin, K. Yao, J. Mater. Sci. 42 (2007) 9205–9209.
[14] L. Song, S. Zhang, B. Chen, J. Ge, X. Jia, Colloids Surf. A, 360 (2010) 1–5.
[15] D.R. Chen, R.R. Xu, J. Solid State Chem. 137 (1998) 185–190.
[16] N. Yanna, P. Zhang, Z. Guo, P. Munroe, H. Liu, Electrochim. Acta 53 (2008) 4213–4218.
[17] F. Geng, Z. Zhao, J. Geng, H. Cong, H.-M. Cheng, Mater. Lett. 61 (2007) 4794–4796.
[18] H.F. Chen, G.D. Wei, X. Han, S. Li, P.P. Wang, M. Chubik, A. Gromov, Z.P. Wang, W. Han, J. Mater. Sci.: Mater. Electron. 22 (2011) 252–259.
[19] G. Sun, B. Dong, M. Cao, B. Wei, C. Hu, Chem. Mater. 23 (2011) 1587–1593.
[20] R.G. Deshmukh, S.S. Badadhe, I.S. Mulla, Mater. Res. Bull. 44 (2009) 1179–1182.
[21] V. Sreeja, P.A. Joy, Mater. Res. Bull. 42 (2007) 1570–1576.
[22] A.P. de Moura, R.C. Lima, M.L. Moreira, D.P. Volanti, J.W.M. Espinosa, M.O. Orlandi, P.S. Pizani, J.A. Varela, E. Longo, Solid State Ionics 181 (2010) 775–780.
[23] H. Ni, Y. Ni, Y. Zhou, J. Hong, Mater. Lett. 73 (2012) 206–208.
[24] S. Komarneni, H. Katsuki, Pure Appl. Chem. 74 (2002) 1537–1543.
[25] P. Benito, M. Herrero, C. Barriga, F.M. Labajos, V. Rives, Inorg. Chem. 47 (2008) 5453–5463.
[26] A.P. de Moura, R.C. Lima, E.C. Paris, M.S. Li, J.A. Varela, E. Longo, J. Solid State Chem. 184 (2011) 2818–2823.
[27] L.S. Cavalcante, J.C. Sczancoski, M.S. Li, E. Longo, J.A. Varela, Colloids Surf. A 396 (2012) 346–351.
[28] S. Komarneni, R. Roy, Q.H. Li, Mater. Res. Bull. 27 (1992) 1393–1405.
[29] M.L. Dos Santos, R.C. Lima, C.S. Riccardi, R.L. Tranquilin, P.R. Bueno, J.A. Varela, E. Longo, Mater. Lett. 62 (2008) 4509–4511.
[30] L.F. da Silva, W. Avansi, M.L. Moreira, A. Mesquita, L.J.Q. Maia, J. Andres, E. Longo, V.R. Mastelaro, J. Nanomater. (2012).
[31] G. Tong, W. Wu, J. Guan, H. Qian, J. Yuan, W. Li, J. Alloys Compd. 509 (2011) 4320–4326.
[32] G.-Y. Zhang, Y.-Y. Xu, D.-Z. Gao, Y.-Q. Sun, J. Alloys Compd. 509 (2011) 885–890.
[33] Q. Hao, S. Liu, X. Yin, Y. Wang, Q. Li, T. Wang, Solid State Sci. 12 (2010) 2125–2129.
[34] L. Diamandescu, D. Mihaila-Tarabasanu, S. Calogero, N. Popescu-Pogrion, M. Feder, Solid State Ionics 101 (1997) 591–596.
[35] H. Jiao, G. Jiao, Mater. Lett. 63 (2009) 2725–2727.
[36] X. Liu, G. Qiu, A. Yan, Z. Wang, X. Li, J. Alloys Compd. 433 (2007) 216–220.
[37] H. Chen, Y. Zhao, M. Yang, J. He, P.K. Chu, J. Zhang, S. Wu, Anal. Chim. Acta 659 (2010) 266–273.
[38] K.J. Rao, B. Vaidhyanathan, M. Ganguli, P.A. Ramakrishnan, Chem. Mater. 11 (1999) 882–895.
[39] T.L. Lai, Y.Y. Shu, G.L. Huang, C.C. Lee, C.B. Wang, J. Alloys Compd. 450 (2008) 318–322.
[40] P.G. Mendes, M.L. Moreira, S.M. Tebcherani, M.O. Orlandi, J. Andres, M.S. Li, N. Diaz-Mora, J.A. Varela, E. Longo, J. Nanopart. Res. 14 (2012).
[41] J.F. Huang, C.K. Xia, L.Y. Cao, X.R. Zeng, Mater, Sci. Eng. B 150 (2008) 187–193.
[42] F.V. Motta, R.C. Lima, A.P.A. Marques, M.S. Li, E.R. Leite, J.A. Varela, E. Longo, J. Alloys Compd. 497 (2010) L25–L28.
[43] D.L.A. de Faria, F.N. Lopes, Vib. Spectrosc. 45 (2007) 117–121.
[44] M. Srivastava, A.K. Ojha, S. Chaubey, J. Singh, P.K. Sharma, A.C. Pandey, J. Alloys Compd. 500 (2010) 206–210.
[45] T.P. Martin, R. Merlin, D.R. Huffman, M. Cardona, Solid State Commun. 22 (1977) 565–567.
[46] D.M. Sherman, T.D. Waite, Am. Mineral. 70 (1985) 1262–1269.
[47] Y.P. He, Y.M. Miao, C.R. Li, S.Q. Wang, L. Cao, S.S. Xie, G.Z. Yang, B.S. Zou, C. Burda, Phys. Rev. B 71 (2005).
[48] C. Xia, W. Ning, Electrochem. Comm. 12 (2010) 1581–1584.
[49] M. Lucero, M. Riquelme, G. Ramirez, M.C. Goya, A.G. Orive, A.H. Creus, M.C. Arevalo, M.J. Aguirre, Int. J. Electrochem. Sci. 7 (2012) 234–250.
[50] A.S. Adekunle, B.O. Agboola, J. Pillay, K.I. Ozoemena, Sens. Actuators B 148 (2010) 93–102.